

Modeling Chemical Vapor Deposition (CVD) Diamond Film Growth with Diamantane-Derived Radicals in Solution: Permissive Evidence in Support of the Garrison–Brenner Mechanism for Incorporation of Carbon into the Dimer Sites of the {100} Diamond Surface

Ken S. Feldman,* Robert F. Campbell, Theodore R. West, Allen D. Aloise, and David M. Giampetro

Department of Chemistry, The Pennsylvania State University, University Park, Pennsylvania 16802

Received July 23, 1999

The synthesis and partial rearrangement of nordiamantanemethyl radical into its more stable diamantyl isomer at 200–300 °C is reported. This solution phase observation attests to the feasibility of similar processes proposed to occur at the surface of {100} diamond film under CVD conditions.

Utilization of chemical vapor deposition (CVD) diamond film in a wide range of emerging technologies that require materials with “extreme” properties ultimately depends on continuing advances in critical process attributes such as film quality, deposition rate, and substrate compatibility. Film quality and quantity concerns have been largely alleviated through exhaustive but strictly empirical optimization studies, although substrate compatibility remains a pressing issue.¹ In recent years, this Edisonian approach has yielded to mechanistic inquiry. Both experimental and computational strategies have been used to probe the gas-phase chemistry and surface structures that define the reaction milieu prior to carbon deposition.² However, investigation of the mechanistic details associated with actual carbon incorporation heretofore has been largely the province of computational chemistry.³ It is plausible that an alternative, experimentally based strategy may provide additional insight into the intimate structural and energetic requirements which attend initiation and propagation of film growth. A model for film growth so developed may

then serve as a platform for initiating new approaches which address the substrate compatibility problem.

Experimental evidence which bears on the overall picture of CVD film growth on the {100} face of diamond was garnered through study of the relationships between various input parameters (gas composition, temperature, pressure, substrate, additives) and the quality and quantity of diamond produced. Optimized protocols typically require a feed gas mixture of 0.2–2% carbon-containing material in H₂ heated to ~2000 °C (microwave, laser, hot filament) passed over a substrate (diamond, silicon, select metals) itself heated to 850–1100 °C. Components of the plasma phase include H₂, H[•], CH₄, CH₃[•], and HC≡CH, and defined roles for H[•] (surface H abstraction, ablating graphitic deposits)^{1c,f} and CH₃[•] (carbon source during growth on the {100} face of diamond)^{2j-n} have been elucidated. STM and AFM studies provide “pictures” of the {100} face of CVD diamond which have been construed as representing a (2 × 1):1H surface reconstruction, **2**, Scheme 1.⁴ Measurement of the overall kinetics of diamond film growth as a function of temperature has permitted calculation of a global Arrhenius activation energy of ~23 kcal/mol ($T \leq 900$ °C).⁵ This value can be interpreted in terms of the calculated barriers for surface H abstraction, whereby two surface C–H bonds (calc. $E_a \approx 10$ kcal/mol each) must be cleaved for incorporation of one epitaxially positioned C atom on

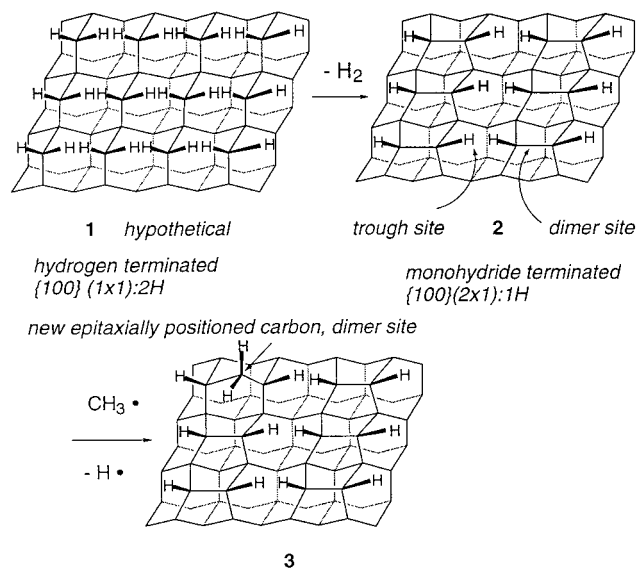
(1) (a) Fields, J. E. *The Properties of Diamond*; Academic Press: London 1979. (b) Bachmann, P. K.; Messier, R. *Chem. Eng. News* **1989**, May 15, 24. (c) Spear, K. E. *J. Am. Ceram. Soc.* **1989**, *72*, 171. (d) Yarbrough, W. A. *J. Am. Ceram. Soc.* **1992**, *75*, 3179. (e) Angus, J. C.; Hayman, C. C. *Science* **1988**, *241*, 913. (f) Yarbrough, W. A.; Messier, R. *Science* **1990**, *247*, 688. (g) Klages, C.-P. *Appl. Phys. A* **1993**, *56*, 513.

(2) (a) Storer, P.; Cai, Y. Q.; Canney, S. A.; Clark, S. A. C.; Khiefets, A. S.; McCarthy, I. E.; Utteridge, S.; Vos, M.; Weigold, E. *J. Phys. D.: Appl. Phys.* **1995**, *28*, 2340. (b) Collins, R. W.; Cong, Y.; Kim, Y.-T.; Vedam, K.; Liou, Y.; Inspektor, A.; Messier, R. *Thin Solid Films* **1989**, *181*, 565. (c) Mori, Y.; Show, Y.; Deguchi, M.; Yagi, H.; Yagyu, H.; Eimori, N.; Okada, T.; Hatta, A.; Nishimura, K.; Kitabatake, M.; Ito, T.; Hirao, T.; Izumi, T.; Sasaki, T.; Hiraki, A. *Jpn. J. Appl. Phys.* **1993**, *32*, 987. (d) Viljoen, P. E.; Roos, W. D.; Swart, H. C.; Holloway, P. H. *Appl. Surf. Sci.* **1996**, *100/101*, 612. (e) Pate, B. B. *Surf. Sci.* **1986**, *165*, 83. (f) Page, M.; Brenner, D. W. *J. Am. Chem. Soc.* **1991**, *113*, 3270–3274. (g) Brenner, D. W. *Phys. Rev. B* **1990**, *42*, 9458. (h) Johnson, C. E.; Weimer, W. A.; Cerio, F. M. *J. Mater. Res.* **1992**, *7*, 1427. (i) Yarbrough, W. A.; Tankala, K.; DebRoy, T. *J. Mater. Res.* **1992**, *7*, 379. (j) Chu, C. J.; D'Evelyn, M. P.; Hauge, R. H.; Margrave, J. L. *J. Appl. Phys.* **1991**, *70*, 1695. (k) Harris, S. J.; Martin, L. R. *J. Mater. Res.* **1990**, *5*, 2313. (l) Chu, C. J.; D'Evelyn, M. P.; Hauge, R. H.; Margrave, J. L. *J. Mater. Res.* **1990**, *5*, 2405. (m) Martin, L. R.; Hill, M. W. *J. Mater. Sci. Lett.* **1990**, *621*. (n) Lee, S. S.; Minsek, D. W.; Vestyck, D. J.; Chen, P. *Science* **1994**, *263*, 1596. (o) Hamza, A. V.; Kubiak, G. D.; Stulen, R. H. *Surf. Sci.* **1990**, *237*, 35.

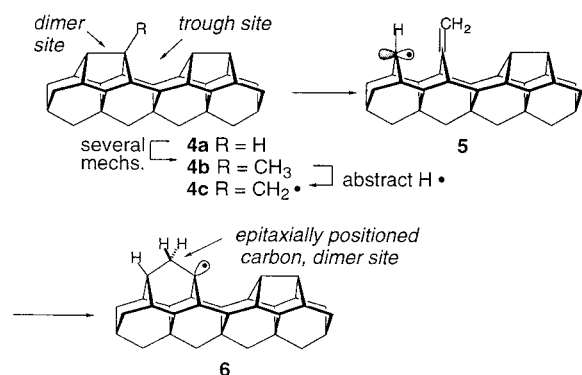
(3) (a) Tsuda, M.; Nakajima, M.; Oikawa, S. *J. Am. Chem. Soc.* **1986**, *108*, 5780. (b) Huang, D.; Frenklach, M. *J. Phys. Chem.* **1992**, *96*, 1868. (c) Skokov, S.; Weiner, B.; Frenklach, M. *J. Phys. Chem.* **1994**, *98*, 7073. (d) Harris, S. J.; Goodwin, D. G. *J. Phys. Chem.* **1993**, *97*, 23. (e) Deak, P.; Giber, J.; Oeschner, H. *Surf. Sci.* **1991**, *250*, 287. (f) Butler, J. E.; Woodin, R. L. *Philos. Trans. R. Soc. London A* **1993**, 209. (g) Musgrave, C. B.; Harris, S. J.; Goddard, W. A., III *Chem. Phys. Lett.* **1995**, *247*, 359. (h) Heggie, M. I.; Jungnickel, G.; Latham, C. D. *Diamond Relat. Mater.* **1996**, *5*, 236. (i) Garrison, B. J.; Dawnkaski, E. J.; Srivastava, D.; Brenner, D. W. *Science* **1992**, *255*, 835. (j) Besler, B. H.; Hase, W. L.; Hass, K. C. *J. Phys. Chem.* **1992**, *96*, 9369. (k) Dawnkaski, E. J.; Srivastava, D.; Garrison, B. J. *J. Chem. Phys.* **1996**, *104*, 5997. (l) Dawnkaski, E. J.; Srivastava, D.; Garrison, B. J. *J. Chem. Phys.* **1995**, *102*, 9401–9411.

(4) (a) Tsuno, T.; Imai, T.; Nishibayashi, Y.; Hamada, K.; Fujimori, N. *Jpn. J. Appl. Phys.* **1991**, *30*, 1063. (b) Sutcu, L. F.; Chu, C. J.; Thompson, M. S.; Hauge, R. H.; Margrave, J. L.; D'Evelyn, M. P. *J. Appl. Phys.* **1992**, *71*, 5930. (c) Sternberg, M.; Frauenheim, Th.; Zimmermann-Edling, W.; Busmann, H.-G. *Surf. Sci.* **1997**, *370*, 232. (5) Kondoh, E.; Ohta, T.; Mitomo, T.; Ohtsuka, K. *J. Appl. Phys.* **1993**, *73*, 3041.

Scheme 1



Scheme 2

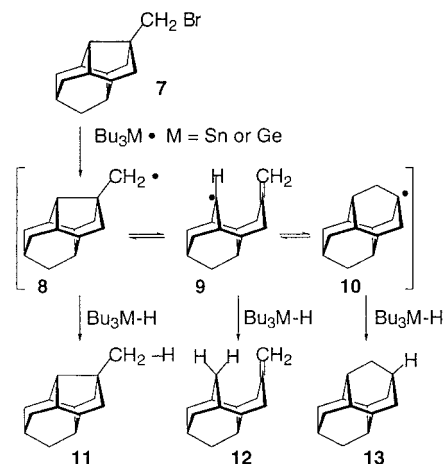


the {100} surface, cf. **1** \rightarrow **3**, Scheme 1.^{2f} The rate of diamond film growth above this temperature regime is mass transfer limited.

One plausible mechanistic proposal for carbon incorporation into a *dimer* site (cf. **2** \rightarrow **3**) has emerged from molecular dynamics simulations.³¹ This mechanism, devised by Garrison and Brenner, is summarized in Scheme 2. The sequence invokes relatively low-energy processes that are well preceded by solution phase hydrocarbon radical chemistry. Facile CH_3 for H exchange at a dimer site (**4a** \rightarrow **4b**) is followed by H^\bullet abstraction to furnish the key cyclopentylmethyl radical **4c** residing on the surface of the diamond lattice. Strain driven β -fragmentation of the stereoelectronically aligned dimer C–C bond in **4c** furnishes the 5-hexenyl-type radical **5**, which can close in a thermodynamically favored (*vide infra*) 6-endo-trig-type cyclization to deliver the epitaxially incorporated carbon in **6**.

Evaluation of this (and other) model(s) of film growth by direct experimental measurement is likely to be thwarted both by the low concentration of reactive species on the diamond surface and by the glowing plasma discharge that attends the CVD process, although some progress in identifying surface-bound species (H and CH_3) by applying second harmonic generation and sum frequency generation techniques to growing diamond film under CVD conditions has been claimed.⁶ On the other hand, the kinetic and thermodynamic properties of the archetypal versions of these radical rearrangements (e.g.,

Scheme 3



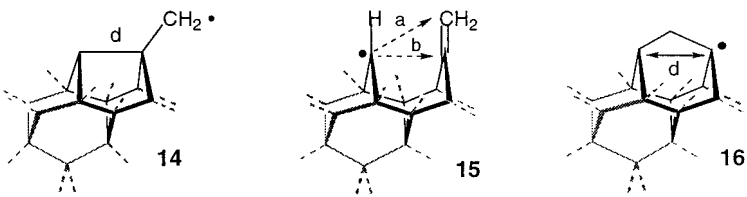
5-hexenyl radical cyclizations/fragmentations) have been thoroughly studied. Bridging the gap between these simple, conformationally mobile radical species and their completely (?) rigid analogues imbedded in a diamond surface, with appropriate partially constrained but synthetically accessible model systems, represents one approach to obtaining permissive evidence which addresses the feasibility of the Garrison–Brenner model. One such model system, based on materially constrained diamantyl constructs, is described herein. The synthesis of a methylordiamantyl radical precursor **8** related to **4c** and a study of its rearrangement to the diamantyl framework **10** (analogous to **4c** \rightarrow **6**) provides insight into the mechanistic model discussed above, Scheme 3.

The validity of this approach to probing mechanistic issues associated with CVD diamond film growth rests on the relevance that small model systems in solution at moderate temperatures (80–300 °C) have to their presumptive analogues at a gas–surface interface under much more extreme conditions (>800 °C). Numerous studies have shown that radical-mediated reactions of simple hydrocarbon species are rather insensitive to milieu and consequently do not display notable variation in kinetic or thermodynamic properties when examined in either nonpolar solvents or in the gas phase.^{3d,7} From this perspective, the extrapolation of conclusions drawn from examination of rearrangements of hydrocarbon radicals in nonpolar solution to similar reactions at the gas–solid interface does not seem unjustified. The striking difference in temperature regimes between the proposed model studies and CVD conditions may be a source of concern, but prior workers have estimated that the activation barriers for the radical rearrangements themselves (e.g., **4c** \rightarrow **5** \rightarrow **6**) are low enough to be surmountable under the lower temperature range examined below (*vide infra*). Speculation about the necessity for temperatures in excess of 800 °C centers on the original surface reconstruction (**1** \rightarrow **2**, Scheme 1).^{2o,3b} Perhaps the most critical assumption in this model study stems from the choice of the carbon framework itself. What type of synthetically accessible structure adequately reflects the restrictions imposed by the crystal-line lattice on the surface feature of interest?

(6) Seki, H.; Yamada, T.; Chuang, T. J.; Chin, R. P.; Huang, J. Y.; Shen, Y. R. *Diamond Relat. Mater.* **1993**, *2*, 567.

(7) (a) Beckwith, A. L. J.; Bowry, V. W.; Ingold, K. U. *J. Am. Chem. Soc.* **1992**, *114*, 4983 and references therein. (b) Kanabus-Kaminska, J. M.; Gilbert, B. C.; Griller, D. *J. Am. Chem. Soc.* **1989**, *111*, 3311.

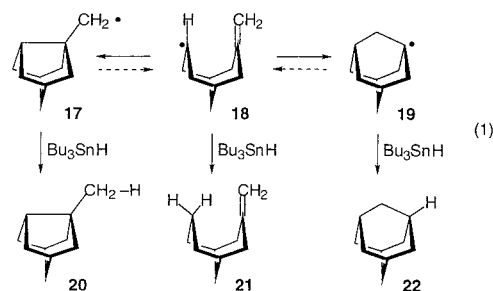
Table 1. Calculated Relative Energies of Radicals 14–16 Contained within Various Sized Frameworks



entry		no. C-atoms	rel. E^{\ddagger} (kcal/mol)	d (Å)	rel. E^{\ddagger} (kcal/mol)	a, b (Å)	rel. E^{\ddagger} (kcal/mol)	d (Å)
Large Clusters								
a	Harris (MM) ^b	330	23.4		28.3		0	
b	Frenklach (PM3) ^c	40, 45	11.6		24		0	
c	Garrison (MD) ^d	256	4.6		6.2		0	
d	this work (PM3)	141	6.1	1.61	16.3	2.84, 2.46	0	2.34
Adamantyl								
e	Chen (MM3/BDE) ^e	10	11		20		0	
f	Chen (6-31G*/MP2) ^f	10	13.9		14.1		0	
g	this work (MM)	10	9.6	1.60	17.1	3.32, 2.87	0	2.45
h	this work (PM3)	10	13.9	1.59	14.1	3.83, 3.17	0	2.39
i	this work (DFT: pBP/DN**)	10	11.9	1.65	15.4	3.57, 2.94	0	2.45
Diamantyl								
j	this work (MM)	14	10.1	1.60	18.9	3.23, 2.77	0	2.45
k	this work (PM3)	14	14.7	1.60	18.6	3.54, 2.87	0	2.39
l	this work (DFT: pBP/DN**)	14	11.1	1.65	16.9	3.52, 2.82	0	2.45

^a Enthalpies of formation are compared for the MM and PM3-based calculations, while total energies are used in the molecular dynamics (MD), ab initio, and density functional calculations. ^b This calculation used both MM3 and MM2 force fields. ^c Reference 3c. ^d The molecular dynamics simulations used a customized force field. ^e This analysis used MM3-based calculations on the parent hydrocarbons less bond dissociation energies of the appropriate C–H bond and the enthalpy of formation of H•. ^f Reference 8.

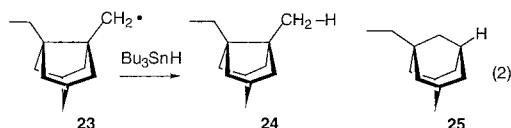
Computational techniques can be utilized to assess the adequacy of putative model compounds for the surface-bound radicals **4c–6**. In fact, prior workers in this area have recorded relative energies of variously sized diamond slab versions of these key species,^{3c,d,i} while Chen and Mueller more recently have documented analogous values for a simple model system based on the adamantyl framework (Table 1).⁸ These studies have been augmented by inclusion of similar computational analyses for the diamantyl-based model system in the current work. The calculated values of the relative enthalpies for radicals **14–16** on the surface of various diamond clusters (Table 1, entries a–d) do not converge. The energy differences appear to be model and/or technique dependent. Therefore, a choice of the “best” representation of the actual diamond surface must be made, and for the purposes of the ensuing discussion, the values obtained when using a medium-sized cluster at the semiempirical level of theory (Table 1, entry d) will be used for comparison (see Supporting Information for Chem 3-D depictions of the 141-carbon models for **14–16**). Calculated relative enthalpies of the adamantyl-based radicals (Table 1, entries e–i) using either semiempirical (SE) (PM3, entry h), ab initio (6-31G*/MP2, entry f), or density functional (DF) (pBP/DN**, entry i) methods provide very similar values. Molecular mechanics (MM) based approaches to the relative enthalpy of these radicals (Table 1, entries e and g) appear to underestimate the energy of **14** (=17, eq 1) and overestimate the energy of **15** (=18, eq 1) relative to the quantum mechanical calculations. The key geometrical parameters noted on the structures **14–16** differ widely among the different calculational techniques. The differences between the MM-, SE-, and DF-based relative energy values within the diamantyl series (cf. **8–10**, Scheme 3) are fairly consistent, with the



notable exception of the PM3-derived energy of **14** (=8). In addition, the key transannular radical–alkene distances in **15** (=9) appear to converge at higher levels of theory, although the other benchmark distances in **14** (=8) and **16** (=10) remain as variable as in the adamantyl series. A comparison of entries h/i and k/l with entry d illustrates both the strengths and weaknesses of claiming that either an adamantyl-based or a diamantyl-based construct system is an acceptable representation of the infinite diamond surface. Given the assumption that the 141-carbon slab in entry d is a fair approximation of the real system, then it is arguable that the diamantyl system is a marginally better representation than the adamantyl lower homologue for the ring-opened radical **15** based upon both relative enthalpies and critical geometrical distances. However, neither the 10-carbon nor the 14-carbon model systems adequately reproduce either the relative energy of the imbedded cyclopentylmethyl radical **14** or the width (d) of the adamantyl fragment of radical **16**. Nevertheless, the diamantyl system is a defensible compromise in light of the intersection between model relevance and ease-of-synthesis considerations.

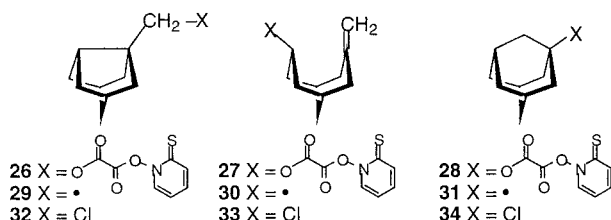
Prior studies on radical rearrangements within the adamantyl system hint at the prospects for detecting the desired conversion of **8** into **10** within the more con-

(8) Mueller, A. M.; Chen, P. *J. Org. Chem.* **1998**, *63*, 4581.



strained diamantyl framework. The seminal work of Lithotrovik et al.⁹ (eq 1) and Yurchenko¹⁰ (eq 2) on the cyclization and rearrangement chemistry, respectively, of adamantyl-related radicals attest to the feasibility of the desired processes. The bicyclo[3.3.1]nonanyl radical **18**, formed by reduction of the corresponding bromide, cyclized through both 5-exo and 6-endo trajectories to furnish an unquantified mixture of the three possible hydrogen trapping products **20–21**. Perhaps more germane is the reported rearrangement of the noradamantylmethyl radical **23**, which delivers the rearranged H-trapping product **25** along with the direct reduction product **24** in unspecified yield, but in ratios suggested to favor rearrangement at higher temperatures.

Scheme 4

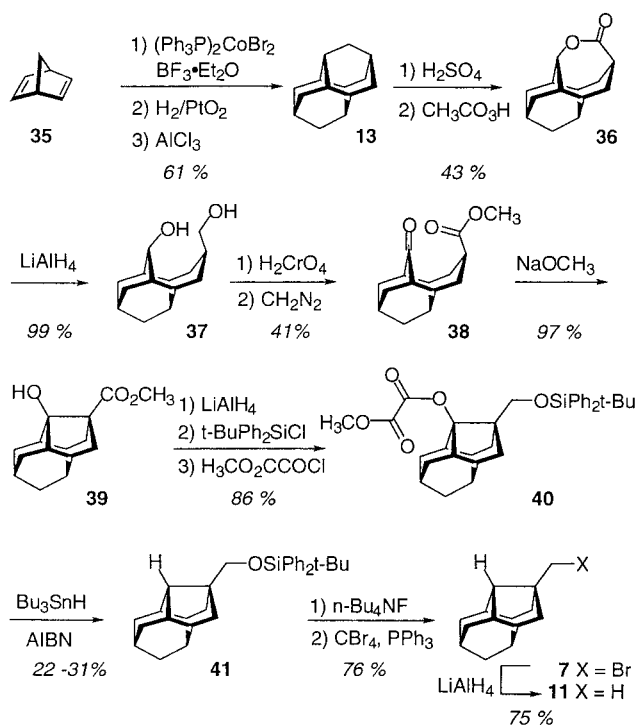


More recently, Chen and Mueller have revisited these adamantyl radical rearrangement processes, quantified kinetic and thermodynamic parameters through a combination of calculation (*vide supra*) and experiment, and interpreted the results in terms of the Garrison–Brenner model for diamond film growth (Scheme 4).⁸ They observed that while the Barton esters **26** and **28** afforded only the unrearranged chlorides **32** and **34**, respectively, upon thermolysis in CCl₄, the bicyclo[3.3.1]nonanyl radical precursor **27** under similar conditions provided mainly the 5-exo closure product **32** along with trace amounts (1–4%) of **33** and **34**. Apparently, fragmentation of radicals **29** and **31** do not compete effectively with chain transfer, although cyclization (**30** → **29**, **30** → **31**) can. The calculated activation barriers for fragmentation of **29** (14.4 kcal/mol), fragmentation of **31** (28.2 kcal/mol), and cyclization of **30** (5.4 and 8.2 kcal/mol) all speak to the facility of these reactions under temperature regimes far lower than that found during CVD diamond film growth. However, the inability to detect the pivotal rearrangement of **29** into **31** may cloud interpretation of these results in the context of the Garrison–Brenner mechanism.

Results and Discussion

The synthesis of bromomethylnordiamantane (**7**) commenced with norbornadiene (**35**), Scheme 5. Following the route developed by McKervey et al.,¹¹ cobalt catalyzed dimerization of **35** followed by hydrogenolysis of the C₁₄H₁₆ dimer and AlCl₃-mediated rearrangement of the

Scheme 5



mixture of hydrogenated products afforded good yields of diamantane (**13**). Sequential oxidations, first with fuming H₂SO₄¹¹ and then with peracetic acid,¹² converted **13** into a 2:1 mixture of lactones. The structure of the major isomer **36** (available in pure form by recrystallization from methanol) was secured by single-crystal X-ray analysis.¹² Reduction of **36** furnished the known diol **37**.¹³ By analogy to chemistry reported in the adamantyl series,¹⁴ oxidation of diol **37** and in situ esterification provided the aldol precursor **38**. Treatment of **38** with base led cleanly to the nordiamantyl β-hydroxyester **39** in nearly quantitative yield. In comparison, the related internal aldol in the adamantyl series afforded the noradamantyl product in only 30% yield along with 70% of recovered uncyclized ketoester at equilibrium.¹⁴ Evidently, the more rigid cage-like structure of the diamantyl system favors transannular cyclization to a significantly greater extent than does the more flexible lower adamantyl homolog. Deoxygenation of the tertiary alcohol in **39** (or a derivative) proved difficult. Eventual recourse to the oxalate **40** sufficed to provide the reduced nordiamantane skeleton **41** in modest yield via radical-mediated reduction. Other radical leaving groups (phenylthiocarbonate, thioxanthate) performed even more poorly, whereas attempts to effect deoxygenation via the methyl oxalate derivative of β-hydroxyester **39** proved fruitless. Perhaps the nonplanar nature of the intermediate tertiary radical derived from **40** contributed to the difficulty of this transformation. Acquisition of the methylnordiamantyl silyl ether **41** permitted uneventful access to the desired bromide **7** following desilylation and bromination via the Lee protocol. Attempts to prepare the iodide analogue of **7** were frustrated by its extreme lability to handling and purification. An authentic sample

(9) Likhovorik, I. R.; Dovgan, N. L.; Barantsova, A. V. *Vestn. Kiev. Politekh. Inst., [Ser.]: Khim. Mashinostr. Tekhnol.* **1981**, *18*, 31.

(10) Yurchenko, A. G. In *Cage Hydrocarbons*; Olah, G. A., Ed.; Wiley and Sons: New York, NY, 1990; p 166.

(11) Courtney, T.; Johnston, D. E.; McKervey, M. A.; Rooney, J. J. *J. Chem. Soc., Perkin Trans. 1* **1972**, 2691.

(12) Ondracek, J.; Janku, J.; Novotny, J.; Vodicka, L.; Csordas, L.; Kratochvil, B. *Collect. Czech. Chem. Commun.* **1989**, *54*, 3260.

(13) Yanku, I.; Golovanyuk, A. N.; Tsybul'ski, A. V.; Vodichka, L.; Yurchenko, A. G.; Iseav, S. D. *J. Org. Chem., USSR* **1990**, *26*, 1180.

(14) Renzoni, G. E.; Borden, W. T. *J. Org. Chem.* **1983**, *48*, 5231.

Table 2. Reduction Products from Combination of Bromide 7 with Bu₃MH (M = Sn or Ge) at Temperatures from 80 to 300 °C

entry	concentration (mM)	metal hydride	temp (°C)	11:13 ^a	yield ^b 11 + 13
a	71	Sn	25		N.R.
b	71	Sn	80	~100:0	95
c	71	Sn	200	~100:0	74
d	71	Sn	300	~100:0	77
e	7	Sn	80	~100:0	84
f	7	Sn	200	~100:0	80
g	71	Ge	80	~100:0	83
h	71	Ge	200	99:1	66
i	71	Ge	300	81:19	56
j	7	Ge	80	98:2	48
k	7	Ge	200	91:9	38
l	7	Ge	300	73:27	5

^a By GC. ^b By GC vs internal standard.

of methylnordiamantane (**11**) was prepared by LiAlH₄-mediated reduction of bromide **7**.

Radical rearrangement studies with bromide **7** were conducted by placing a sealed, evacuated, heavy-walled glass tube containing the bromide, 0.5 equiv AIBN and 1.2–1.5 equiv of Bu₃MH (M = Sn or Ge) in solvent (PhH or *o*-C₆H₄Cl₂) into an oil bath preheated to the indicated temperature. After 45 min (300 °C) or 1 h (80, 200 °C), the solution was cooled to room temperature and assayed by GC. The ratios of observed products **11** and **13** (Scheme 3) were determined by integration of the GC trace and corrected for detector response by comparison to a calibration curve constructed from mixtures of known concentrations of **11** and **13**. The absolute yields of **11** and **13** were determined by GC analysis of a measured aliquot of the crude reaction mixture spiked with a known quantity of the internal standard *n*-nonane (detector response corrected by a standard calibration curve). Control experiments established that (1) bromide **7** did not react in any fashion prior to high-temperature exposure, and (2) the products did not equilibrate or decompose under the reaction conditions. Workup and chromatographic analysis of the crude reaction mixtures did not afford any characterizable material in addition to **11** and **13**. Unidentified decomposition products of **7** presumably account for the remainder of the unrecovered mass, a point which cautions against overinterpretation of those experiments where the yields of **11** and **13** are quite low. Two concentrations were explored (71 and 7 mM), as were both relatively good (Bu₃SnH) and relatively poor (Bu₃GeH) hydrogen donors in an effort to preserve the lifetime of radical **8** long enough to participate in rearrangement. The results of these experiments are tabulated above.

An examination of these data reveal that no conditions employing Bu₃SnH as the hydrogen donor could be identified that permitted detection of the rearrangement of radical **8** into **9** or **10**. Switching to the slower hydrogen donor Bu₃GeH afforded results that were more promising. In these series (Table 2, entries g–l), small quantities of the rearranged product **13** could be detected in almost all runs. Both higher dilution (Table 2, entry k vs h) and higher temperature (Table 2, entries i and l vs g/h and j/k, respectively) favored formation of **13** relative to **11**. In no instance was any evidence (¹H NMR) for the ring-opened product **12** forthcoming. In contrast, Chen and Mueller, when starting with the ring-opened radical precursor **27**, observed small amounts of the ring-opened product **33** in the adamantyl series. These seemingly

contradictory observations are not entirely unexpected in light of the facile aldol cyclization of **38** vis-à-vis its lower adamantyl homolog. Unfortunately, the lack of any observable **12** formation defeats attempts to determine rate constants from the product distribution data. Nevertheless, the qualitative observation that the diamantyl product **13** is formed from rearrangement of the initial nordiamantylmethyl radical **8** provides additional experimental support for the key carbon incorporation steps proposed by Garrison and Brenner in their diamond film growth model.

Experimental Section

Moisture- and oxygen-sensitive reactions were carried out in flame-dried glassware under an Ar atmosphere. Tetrahydrofuran (THF) was distilled from sodium benzophenone ketyl under an Ar atmosphere immediately before use. Toluene, benzene (C₆H₆), and dichloromethane (CH₂Cl₂) were distilled from calcium hydride (CaH₂) under an Ar atmosphere immediately before use. Purification of products via flash chromatography¹⁵ was performed with 32–63 mm silica gel and the solvent systems indicated. Hexane and diethyl ether (Et₂O) used in flash chromatography were distilled from CaH₂ prior to use, whereas ethyl acetate (EtOAc) was used as purchased. Melting points are uncorrected. Chemical impact mass spectra (MS) were obtained with isobutane as the reagent gas. Combustion analyses were performed by either Galbraith Laboratories, Knoxville, TN or Midwest Microlab, Indianapolis, IN. AIBN was recrystallized from absolute ethanol. Bu₃SnH and Bu₃GeH were distilled prior to use and stored under nitrogen. Gas chromatograph based yields were determined on a gas chromatograph equipped with a methyl silicon capillary column and a flame ionization detector. Copies of ¹H and ¹³C NMR spectra are provided in the Supporting Information to establish purity for those compounds that were not subject to combustion analyses.

Ketoester 38. Diol **37**¹³ (2.50 g, 11.3 mmol) was suspended in 170 mL acetone and cooled in an ice bath. A solution of CrO₃ (5.65 g, 56.5 mmol, 5 equiv) in 5.7 mL of concentrated H₂SO₄ and 23 mL of water was added dropwise over 2 h to this stirring suspension. The solution was allowed to warm to room temperature and stirred for an additional 5 h. The solution was diluted with 100 mL of Et₂O and poured into brine. The mixture was extracted with Et₂O and the combined organic phases were washed with brine. The organic phase was concentrated to 150 mL and extracted with saturated NaHCO₃. The aqueous phase was acidified with 50% H₃PO₄, extracted with CH₂Cl₂, dried with Na₂SO₄, filtered, and concentrated. The resulting white solid was redissolved in 20 mL of CH₂Cl₂ and treated with ethereal CH₂N₂ until a yellow color persisted. Excess CH₂N₂ was destroyed by addition of 1 mL of glacial HOAc. The solution was concentrated in vacuo, and the resulting oil was purified by silica gel chromatography (50% EtOAc/Hexane) to provide a yellow oil that solidified on standing to afford **38** (1.51 g) as a yellow solid (41%). mp 51–52 °C; IR (CCl₄) 1724 cm⁻¹; ¹H NMR (200 MHz, CDCl₃) δ 3.66 (s, 3 H), 2.53 (t, *J* = 7.47 Hz, 1 H), 2.40 (s, 4 H), 2.12–1.79 (m, 12 H); ¹³C NMR (90 MHz, CDCl₃) δ 218.3, 175.2, 53.2, 51.6, 40.5, 40.2, 36.5, 33.9, 30.9, 29.9, 26.1; MS *m/z* (relative intensity) 248 (M⁺, 100); Anal. Calcd for C₁₅H₂₀O₃: C, 72.55; H, 8.12. Found: C, 72.51; H, 8.14.

β-Hydroxyester 39. Ketoester **38** (1.15 g, 4.64 mmol) was dissolved in 13 mL of CH₃OH and purged with Ar. To this solution was added sodium methoxide (0.065 g, 1.20 mmol) in 3 mL of CH₃OH via syringe. The solution was stirred at room temperature for 4 h at which time TLC indicated complete consumption of starting material. The solution was poured into 80 mL of Et₂O and acidified with 1 M H₃PO₄. The organic layer was washed with brine, dried with Na₂SO₄, filtered, and concentrated to give **39** (1.12 g) as a white crystalline solid

(97%). mp 121–123 °C; IR (CCl₄) 3587, 1712 cm⁻¹; ¹H NMR (200 MHz, CDCl₃) δ 3.71 (s, 3 H), 2.90 (s, 1 H), 2.28–1.60 (m, 16 H); ¹³C NMR (50 MHz, CDCl₃) δ 176.1, 85.0, 55.9, 51.6, 48.1, 43.8, 43.1, 34.3, 33.8, 30.6, 24.4; MS *m/z* (relative intensity) 248 (M⁺, 16.3); HRMS calcd for C₁₅H₂₀O₃ 248.1412, found 248.1428.

Oxalate 40. Ester **39** (3.70 g, 14.8 mmol) was dissolved in 100 mL of Et₂O and transferred via cannula to a suspension of LiAlH₄ (0.731 g, 19.2 mmol) in 62 mL of Et₂O. The mixture was stirred at room temperature for 5 h, and the excess hydride was destroyed by dropwise addition of EtOAc. The mixture was poured into 200 mL of 10% aqueous Rochelle's salt and extracted with CHCl₃. The organic phase was dried with Na₂SO₄, filtered, and concentrated to afford 3.23 g of a white solid (92%). An analytical sample of the resulting diol was prepared by recrystallization from CHCl₃, mp 154–156 °C; IR (KBr) 3283 cm⁻¹; ¹H NMR (360 MHz, d-6 DMSO) δ 4.39 (d, *J* = 1.84 Hz, 1 H), 3.99 (td, *J* = 5.54, 1.83 Hz, 1 H), 3.36 (d, *J* = 5.52 Hz, 2 H), 1.95–1.30 (m, 16 H); ¹³C NMR (90 MHz, CDCl₃) δ 83.5, 66.1, 50.3, 49.1, 43.2, 42.7, 35.0, 34.6, 30.8, 24.7; MS *m/z* (relative intensity) 202 (M⁺-H₂O, 100). Anal. Calcd for C₁₄H₂₀O₂: C, 76.33; H, 9.15. Found: C, 76.23; H, 9.10. This diol (0.919 g, 3.86 mmol) and imidazole (0.919 g, 13.5 mmol) were mixed in 3 mL of DMF and purged with Ar. *tert*-Butylchlorodiphenylsilane (1.11 g, 4.05 mmol) was added dropwise via syringe and the solution was stirred at room temperature for 12 h. The reaction mixture was then diluted with Et₂O (100 mL) and washed with 1 M H₃PO₄ and water. The organic phase was dried with Na₂SO₄, filtered, and concentrated to give a yellow oil which was chromatographed on silica gel (4% EtOAc in hexane) to afford the monoprotected diol (2.72 g) as a colorless oil (97%). IR (CCl₄) 3548 cm⁻¹; ¹H NMR (200 MHz, CDCl₃) δ 7.71–7.66 (m, 4 H), 7.42–7.35 (m, 6 H), 3.70 (s, 2 H), 3.37 (s, 1 H), 2.03–1.64 (m, 14 H), 1.28–1.23 (m, 2 H), 1.07 (s, 9 H); ¹³C NMR (50 MHz, CDCl₃) δ 135.5, 132.7, 129.7, 127.7, 83.0, 67.0, 50.4, 49.2, 43.2, 42.7, 35.0, 34.6, 31.0, 26.9, 24.7, 19.2; MS *m/z* (relative intensity) 459 (MH⁺, 15), 401 (M⁺-*t*-Bu, 99), M⁺-TBDPS, 100). Anal. Calcd for C₃₀H₃₈O₂Si: C, 78.55; H, 8.35. Found: C, 78.45; H, 8.29. This monoprotected alcohol (3.85 g, 8.07 mmol) and DMAP (1.58 g, 13.0 mmol) were mixed in 45 mL of CH₂Cl₂. The suspension was purged with Ar and methyl oxalyl chloride (6.28 g, 51.1 mmol) was added dropwise via syringe. The solution was stirred at room temperature for 6.5 h at which time all the starting material had been consumed (TLC). The solution was diluted with 150 mL of Et₂O and washed with 1 M H₃PO₄ and brine. The organic phase was dried with Na₂SO₄, filtered, and concentrated. Silica gel chromatography of the residue (15% EtOAc/Hexane) afforded 4.40 g of oxalate **40**, a white solid (96%). mp 113–114 °C; IR (CCl₄) 1771, 1743 cm⁻¹; ¹H NMR (200 MHz, CDCl₃) δ 7.65–7.61 (m, 4 H), 7.40–7.24 (m, 6 H), 3.74 (s, 3 H), 2.76 (s, 2 H), 2.05–1.67 (m, 14 H), 1.44–1.39 (m, 2 H), 1.03 (s, 9 H); ¹³C NMR (50 MHz, CDCl₃) δ 158.7, 156.8, 135.7, 133.8, 129.4, 127.5, 94.8, 66.8, 53.4, 53.0, 45.4, 44.0, 43.0, 34.6, 34.4, 30.8, 26.9, 24.2, 19.4; MS *m/z* (relative intensity) 545 (MH⁺, 8.8), 467 (M⁺-Ph, 12.5). Anal. Calcd for C₃₃H₄₀O₅-Si₅: C, 72.75; H, 7.40. Found: C, 72.70; H, 7.47.

Tributyltin Hydride Reduction of Oxalate 40. Oxalate **40** (4.0 g, 7.4 mmol) was dissolved in 160 mL of toluene and purged with Ar via two freeze–pump–thaw cycles. The solution was heated to reflux and Bu₃SnH (7.0 mL, 26 mmol) was added via syringe. AIBN (2.18 g, 13.3 mmol) was dissolved in 40 mL of toluene and purged with Ar as above. The AIBN solution was then added to the refluxing oxalate solution over 6 h and the reaction mixture was allowed to reflux for one additional hour. At that time, the solution was concentrated in vacuo and chromatographed (100% hexane) to afford 713 mg of **41** as a colorless oil (22%). ¹H NMR (200 MHz, CDCl₃) δ 7.69–7.65 (m, 4 H), 7.38–7.36 (m, 6 H), 3.62 (s, 2 H), 1.99–

1.45 (m, 17 H), 1.06 (s, 9 H); ¹³C NMR (50 MHz, CDCl₃) δ 135.7, 134.2, 129.4, 127.5, 69.2, 52.9, 45.6, 44.8, 44.7, 41.9, 36.0, 35.0, 33.8, 26.9, 25.1, 19.5; MS *m/z* (relative intensity) 442 (M⁺, 0.1), 385 (M⁺-*t*-Bu, 100); HRMS calcd for C₃₀H₃₈OSi 442.2692, found 442.2721.

Bromomethylnordiamantane (7). To the protected alcohol **41** (0.713 g, 1.6 mmol) was added *n*-Bu₄NF (24.0 mL of a 1 M solution in THF, 24.0 mmol) via syringe. The solution was purged with Ar and stirred at room temperature for 8 h, at which time the reaction mixture was poured into 200 mL of Et₂O and the organic phase was washed consecutively with 1 M H₃PO₄ and water. The organic phase was dried with Na₂SO₄, filtered, and concentrated to give a white solid which was purified by silica gel chromatography (15% EtOAc/Hexane) to afford 311 mg of the free alcohol as a white solid (95%). mp 118–120 °C; IR (CCl₄) 3637 cm⁻¹; ¹H NMR (360 MHz, CDCl₃) δ 3.61 (s, 2 H), 1.96–1.51 (m, 17 H); ¹³C NMR (90 MHz, CDCl₃) δ 68.9, 52.7, 45.4, 44.6, 44.4, 41.9, 35.7, 34.8, 33.6, 24.8; MS *m/z* (relative intensity) 204 (M⁺, 4). This alcohol (311 mg, 1.5 mmol) and PPh₃ (519 mg, 2.0 mmol) were mixed and dissolved in 13 mL of THF. The mixture was purged with Ar and cooled in a cold water bath. A solution of CBr₄ (657 mg, 2.0 mmol) dissolved in 6 mL of CH₃CN was added dropwise via syringe and the reaction was stirred for 14 h at room temperature under Ar. At that time, the reaction mixture was concentrated and the residue was chromatographed on silica gel (100% hexane) to afford 321 mg of **7** as a white solid (80%). mp 49–50 °C; ¹H NMR (300 MHz, C₆D₆) 3.29 (s, 2 H), 1.84–1.51 (m, 17 H); ¹³C NMR (90 MHz, C₆D₆) δ 52.5, 47.4, 47.2, 46.5, 43.8, 42.4, 35.9, 35.3, 34.1, 25.2; MS *m/z* (relative intensity) 187 (M⁺-Br, 40); Anal. Calcd for C₁₄H₁₉Br: C, 62.93; H, 7.17; Br, 29.90. Found: C, 62.79; H, 7.17; Br, 30.16.

Methylnordiamantane (11). Bromide **7** (200 mg, 0.75 mmol) was dissolved in 2 mL of THF, purged with Ar, and added to an Ar-purged suspension of LiAlH₄ (28 mg, 0.75 mmol) in 10 mL of THF. The suspension was refluxed for 24 h, and excess LiAlH₄ was destroyed by dropwise addition of EtOAc. The mixture was poured into 25 mL of 10% aqueous Rochelle's salt, extracted with ether, and washed with brine. The organic phase was dried with Na₂SO₄, filtered, and concentrated. The resulting solid was purified by silica gel chromatography (100% hexane) to afford 105 mg of **11** as a white solid (75%). mp 78–79 °C; IR (CCl₄) 2907 cm⁻¹; ¹H NMR (C₆D₆, 300 MHz) δ 1.83–1.44 (m, 17 H), 1.17 (s, 3 H); ¹³C NMR (C₆D₆, 100 MHz) δ 50.8, 49.4, 47.2, 47.1, 42.9, 36.0, 35.9, 34.8, 26.4, 26.1; MS *m/z* (relative intensity) 188 (M⁺, 100). Anal. Calcd for C₁₄H₂₀: C, 89.29; H, 10.71. Found: C, 89.68; H, 10.61.

General Procedure for the Bu₃MH-Mediated Reduction of Bromide 7. Bromide **7** was dissolved in benzene (or *o*-dichlorobenzene for the 300 °C runs) to give a concentration of either 7 or 71 mM. To this solution was added either Bu₃-SnH or Bu₃GeH (1.5 equiv) followed by AIBN (0.5 equiv). The solution was deoxygenated with two freeze–pump–thaw cycles and sealed under vacuum. This room temperature solution was then plunged into a preheated oil bath at the indicated temperature. After 1 h (45 min for the 300 °C runs), the crude reaction mixture was analyzed by GC-MS as described.

Acknowledgment. We thank the National Science Foundation (CHE9727305) for financial support.

Supporting Information Available: Copies of ¹H and ¹³C NMR spectra for **39** and **41** and PM3-derived Chem3D depictions of the 141-carbon cluster versions of radicals **14**–**16**. This material is available free of charge via the Internet at <http://pubs.acs.org>.

JO9911793